Angell plot from the potential energy landscape perspective

D. M. Zhang [1], D. Y. Sun,[2,3] and X. G. Gong[1,3]

[1]*Key Laboratory for Computational Physical Sciences (MOE), Institute of Computational Physics, Fudan University, Shanghai 200433, China*

[2]*Engineering Research Center for Nanophotonics & Advanced Instrument (MOE), School of Physics and Electronic Science, East China Normal University, 200241 Shanghai, China*

[3]*Shanghai Qi Zhi Institution, Shanghai 200030, China*

Within the scenario of the potential energy landscape (PEL), a thermodynamic model has been developed to uncover the physics behind the Angell plot. In our model, by separating the barrier distribution in PELs into a Gaussian-like and a power-law form, we obtain a general relationship between the relaxation time and the temperature. The wide range of the experimental data in the Angell plot, as well as the molecular-dynamics data, can be excellently fitted by two characteristic parameters, the effective barrier (ω) and the effective width (σ) of a Gaussian-like distribution. More importantly, the fitted ω and σ^2 for all glasses are found to have a simple linear relationship within a very narrow band, and fragile and strong glasses are well separated in the ω-σ^2 plot, which indicates that glassy states appear only in a specific region of the PEL.

I. INTRODUCTION

The Angell plot (AP) [1], depicting the α-relaxation time (τ_α) as a function of the reciprocal temperature [in units of the glass transition temperature (T_g)] is a very important plot in the research field of glasses. The fragility, a key concept of glasses, defined as $m = \frac{d\log(\tau_\alpha)}{d(T_g/T)}|_{T=T_g}$, can directly be visualized in an AP. Fragility then lets us divide glasses into two classes: strong and fragile. For strong glasses, τ_α can be roughly fitted by the Arrhenius equation in the range between the melting temperature and T_g, while for a fragile glass, τ_α shows a non-Arrhenius behavior (usually referred to as super-Arrhenius) [2–4]. The most essential scientific significance of the AP may be as a general classifier among various glass-forming materials [4]. For this reason, it is believed that the AP must deeply relate to the intrinsic nature of glasses.

Over past decades, great efforts have been made to look for the physical interpretation of the AP. These studies span from theoretical models to computer simulations [5–36]. Among them, the potential energy landscape (PEL) provides a *first-principles* perspective for exploring the physics behind the AP, in which the relation between the statistical properties of PELs and the fragility is thought to be a central issue. The PEL scenario of glasses comes from Goldstein's seminal paper published a half century ago [37]. Since then, it is generally believed that the PEL is indeed a very useful perspective, which can be used to investigate various glass-related problems [38–43]. Up to now, some possible connections between the PEL and the AP have been suggested. For existing models, difficulty is met when one tries to unify strong and fragile glasses within the same framework. For example, as a typical PEL-based model, the Gaussian model predicts a quadratic dependence of τ_α on temperature [13], and the quadratic form well describes both strong and weak fragile glasses. However,

if the quadratic form is used to fit typical fragile glasses, a negative average barrier emerges, which is obviously nonphysical. Elmatad, Chandler, and Garrahan (ECG) have used the quadratic form within a class of kinetically constrained consideration [9]. The ECG model does avoid the nonphysical negative barrier, but it encounters other problems for strong glasses (see below for details).

In spite of great efforts, the physics underlying the AP is not yet well understood, and a unified picture for both strong and fragile glasses is still missing. In this paper, we present a unified PEL model for α relaxation in both strong and fragile glasses using two basic facts: the existence of the barrier distribution in the PEL, and the Arrhenius relationship for a single relaxation event. The current model cannot only well establish the quantitative link between PELs and the AP, but also predicts a general relationship to classify strong and fragile glasses.

II. PEL MODEL

A. Mathematical derivation

It is generally recognized that the existence of metabasins (MBs) is a significant feature of PELs for glass-forming liquids [44,45]. A basin is a region of minima in the PEL with similar potential energies. They are thought to be organized into groups, and form MBs, which have been identified in a few molecular dynamics (MD) simulations and experimental studies [46–48]. Since the α relaxation is related to the transition between MBs [49,50], we will limit our discussion to the inter-MB relaxation. The PEL of a real glass-forming system may be composed of a large number of MBs or different relaxation channels. However, the overall relaxation time of the system must be contributed by all MBs or channels, which is actually the relaxation time measured by experi-
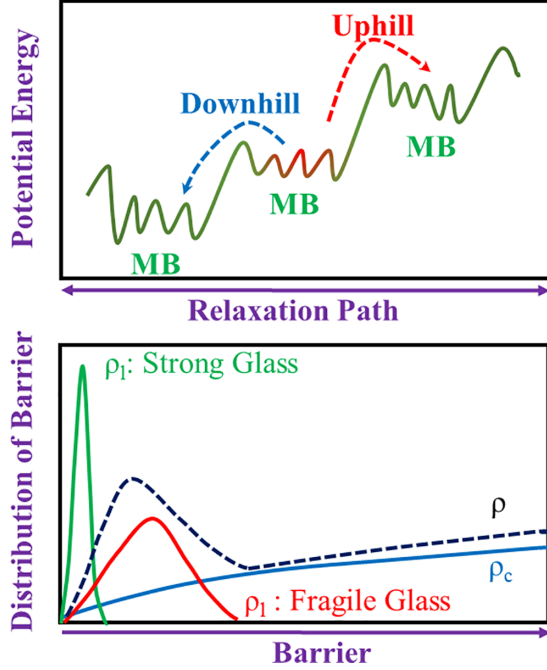
FIG. 1. Upper panel: Schematic plot of metabasins (MB) and possible relaxation paths. Lower panel: Possible shapes of the barrier distribution. The total distribution of barriers $\rho(x)$ is divided into two parts: the distribution mainly coming from downhill relaxations $\rho_l(x)$ and that from uphill relaxations $\rho_c(x)$. For a given $\rho_c(x)$ (blue solid line), the possible $\rho_l(x)$ for the strong and fragile glass are plotted in green and red, respectively.

ments. Our model considers the relaxation of the system as a whole rather than any specific MB. In the current model, at the dynamic level, the only assumption is the validity of the Arrhenius relation for *a single relaxation event*, which is also a general consensus in studying the dynamics of glasses [8,51,52]. Based on the discussion above, our model does not make any specific assumptions about whether the system is in equilibrium. The goal of our model is to establish the link between a given PEL and the temperature dependence of the relaxation time.

To illustrate our model, consider a system currently staying in a MB, in which there are many paths connecting to other MBs as schematically shown in Fig. 1. Clearly, the number of paths is closely related to the local configuration entropy. Define a function $\rho(x)$, which counts the number of paths with the barrier x. Hereafter $\rho(x)$ is called the distribution of barriers (DOB). Since the system will try each path with an equal probability, a single jump can be described by the Arrhenius formula, and the average α-relaxation time (τ_α) is

$$\frac{1}{\tau_\alpha} = \frac{1}{\tau_0} \int \rho(x) e^{-\beta x} dx, \qquad (1)$$

where τ_0 and β are the characteristic timescale and reciprocal temperature, respectively. Since our model is developed for the relaxation of the system as a whole rather than for a specific MB, $\rho(x)$ should be considered as the overall distribution of the relaxation channels. It needs to be pointed out that Eq. (1) implies the relaxation of the overall system resulting from a superposition of many local or nonlocal processes.

For a given path, we label the average potential energy of the initial and final states of system as E_i and E_f, respectively. For the *uphill relaxation* (see Fig. 1), as the difference between E_i and E_f is large, it is a good approximation to write $x \approx E_f - E_i$. With this approximation, the DOB for larger barriers [$\rho_c(x)$] should be $\rho_c(x) \approx \Omega(E_f) \approx \Omega(E_i + x)$, in which $\Omega(E_f)$ corresponds to the number of states with a potential energy of E_f. Clearly $k_B \ln[\Omega(E_f)]$ is nothing but the configurational entropy at fixed potential energy E_f. Because the entropy is an extensive quantity, the leading term of $\Omega(E)$ may have the form, as discussed in many texts [53], $R_c \left(\frac{x + E_i - E_0}{N} \right)^{B_c N}$, where R_c and B_c are material-dependent constants. E_0 is the true ground-state energy of the system (*note:* not the energy of glass at zero temperature). Finally,

$$\rho_c(x) = R_c \left(\frac{x + E_i - E_0}{N} \right)^{B_c N} = R_c e^{g(x)}. \qquad (2)$$

The above equation can be obtained according to the definition of entropies; the detailed mathematical derivation is presented in Appendix A. Regarding Eq. (2), two points should be made. (i) It meets the physical requirement that entropy is an extensive quantity, and entropy will not change with the translation of energy as a whole. A similar consideration, namely, the entropy being additive, has been used to analyze possible formulas for the density of states [54–57]. (ii) Equation (2) may include only the leading term, which refers to the formula in the thermodynamic limit ($N \to \infty$). For practical systems, $g(x)$ may contain other similar power terms, but this does not affect our discussion other than increasing mathematical complexity. The long tail of high energies found in some papers may relate to this kind of distribution [19,28,58–60].

For *downhill relaxations*, the barrier usually does not correlate to the energy of the final states and will distribute in a narrow region. Physically, downhill DOB should approach zero for both large and small x, which is schematically shown in the lower panel of Fig. 1 (blue or red lines). If $\rho_l(x)$ is used to describe the DOB of downhill relaxation, the total DOB $\rho(x) = \rho_l(x) + \rho_c(x)$.

It needs to be stressed that if the barrier x is smaller or comparable to $E_f - E_i$, the above approximation for $\rho_c(x)$ may not be appropriate. Physically, $\rho_c(x)$ should be zero for x less than a certain positive value and may not be a smooth function as is Eq. (2) for small x. Here for mathematical convenience, we still define $\rho_c(x)$ in the range of $[0 : \infty]$ and incorporate the corresponding correction into $\rho_l(x)$. With this correction, $\rho_l(x)$ and $\rho_c(x)$ do not come purely from downhill and uphill relaxation, respectively. However, we still name $\rho_l(x)$ and $\rho_c(x)$ for the DOBs for downhill and uphill relaxations, respectively.

In real materials, $\rho_l(x)$ may contain multiple maxima; in order to keep the form concise, only one dominant maximum is considered. For real systems, we can always write it as the sum of a few functions, each containing a single maximum. The final mathematical form should not change with the number of maxima. Without losing generality, we rewrite $\rho_l(x)$ as $R_l e^{-f(x)}$ with $f(x) \geqslant 0$. Further, we can express $f(x)$ as a polynomial, namely, $f(x) = \sum_{i=0}^{M} a_i x^i$. Based on the above assumptions, $\rho_l(x)$ has a single maximum, as does

$f(x)$. Assuming the maximum appears at x_0, mathematically, there will always exist n_M and n_m to make $A(x - x_0)^{n_M} \geqslant f(x) \geqslant a(x - x_0)^{n_m}$ true for any x. For the convenience of mathematical analysis and keeping major physics unchanged, we take the form $f(x) = B_l(x - \Delta)^n$, where B_l, R_l, Δ, and n are constants larger than zero. By properly choosing the values of B_l, R_l, Δ, and n, $f(x)$ can roughly describe a specific system.

Considering $\rho(x) = \rho_l(x) + \rho_c(x)$, Eq. (1) becomes

$$\frac{1}{\tau_\alpha} = \frac{1}{\tau_l} + \frac{1}{\tau_c}, \tag{3a}$$

with

$$\frac{1}{\tau_l} = \frac{1}{\tau_0} \int \rho_l(x) e^{-\beta x} dx = \frac{R_l}{\tau_0} \int e^{-\beta x - f(x)} dx \tag{3b}$$

and

$$\frac{1}{\tau_c} = \frac{1}{\tau_0} \int \rho_c(x) e^{-\beta x} dx = \frac{R_c}{\tau_0} \int e^{-\beta x + g(x)} dx. \tag{3c}$$

Both $e^{-\beta x - f(x)}$ and $e^{-\beta x + g(x)}$ should be fast-decaying functions of x. Namely it is important only in the vicinity of the maximum of $-\beta x - f(x)$ and $-\beta x + g(x)$. After some mathematical deductions (see Appendixes B and C for details), we reach the final results,

$$\frac{1}{\tau_l} \approx \frac{R_l}{\tau_0} \sqrt{\frac{2\pi}{f''(\bar{x})}} e^{-\frac{\Delta}{k_B T} - (n-1) B_l \left(\frac{1}{n B_l k_B T}\right)^{\frac{n}{n-1}}} \tag{4}$$

and

$$\frac{1}{\tau_c} \approx \frac{R_c}{\tau_0} \sqrt{\frac{2\pi}{|g''(\bar{x})|}} e^{\frac{E_i}{k_B T} - \frac{E_0}{k_B T} + B_c N + B_c N \ln\left(\frac{B_c N}{\mathbb{N}\beta}\right)}. \tag{5}$$

In order to further simplify the mathematics, we keep only the first two leading terms, which change fastest with temperature. In Eqs. (4) and (5), besides those explicitly containing temperature, E_i is also a function of temperature, which is the average potential energy of systems at the current temperature, similar to the configurational energy (total energy minus vibrational energy) [43]. E_i must be a monotonically increasing function of temperature, because the derivative of energies over temperature is the specific heat. In the temperature range focused on in the current work, quantum effects can be neglected, and the change of energy with temperature should be very close to linear. E_i may be approximated as $\sim \in_0 + \in_1 T + O(T)$ (here $\in_0$ and $\in_1$ are constants for a given system, and $\in_0$ is the energy of the glasses at zero temperature). Here $O(T)$, which counts those terms changing slowly with temperature, is neglected. The last term in the exponential function of Eq. (5), $B_c N \ln(\frac{B_c N}{\mathbb{N}\beta}) \propto g(\bar{x})$, is proportional to the configuration entropy, since $R_c e^{g(\bar{x})}$ is the number of configurations. The dependence of entropy on temperature is much weaker than that of energy, since $T\frac{dS}{dT} = \frac{dE}{dT} = C$ with C being the specific heat. For example, the entropy of a binary Lennard-Jones glass is about $T^{0.4}$ [61] and is similar in other glasses [62]. Considering the above arguments, Eqs. (4) and

(5) become

$$\frac{1}{\tau_l} \approx \frac{1}{\bar{\tau}_l} e^{-\frac{\omega_l}{k_B T} - \left(\frac{\sigma_l}{k_B T}\right)^{n_l}} \tag{6}$$

and

$$\frac{1}{\tau_c} \approx \frac{1}{\bar{\tau}_c} e^{-\frac{\omega_c}{k_B T}}. \tag{7}$$

As an approximation, here the constants and the part slowly changing with temperature in Eqs. (4) and (5) are collected into two new constants, $\bar{\tau}_l$ and $\bar{\tau}_c$, respectively. According to our definition, $\omega_l = \Delta > 0$, and $\omega_c = E_0 - \in_0$ is the difference between the ground-state energy of systems E_0 and the zero-temperature energy of the glass $\in_0$. For almost all vitrification process, $\in_0$ is higher than E_0, and obviously $\omega_c \leqslant 0$. $\sigma_l = (n-1)^{\frac{n-1}{n}} \frac{n}{\sqrt[n]{B_l}}$ measures the effective width of the downhill distribution ρ_l. According to our analysis in Appendix B, n_l must be less than or equal to 2 due to $n_l = \frac{n}{n-1} \leqslant 2$. $n_l = 2$ corresponds to $\rho_l(x)$ being a Gaussian distribution.

To calculate the total relaxation time τ_α determined by Eqs. (3), we consider three cases. First, if $\tau_l \ll \tau_c$, then $\tau_\alpha \approx \tau_l$. We have

$$\ln \tau_\alpha \approx \ln \bar{\tau}_l + \frac{\omega_l}{k_B T} + \left(\frac{\sigma_l}{k_B T}\right)^{n_l}. \tag{8a}$$

Second, if $\tau_l \gg \tau_c$, then $\tau_\alpha \approx \tau_c$, we have

$$\ln \tau_\alpha \approx \ln \bar{\tau}_c + \frac{\omega_c}{k_B T}. \tag{8b}$$

Third, if $\tau_l \sim \tau_c$, $\frac{1}{\tau_\alpha} = \frac{1}{\tau_l} + \frac{1}{\tau_c} \approx 2\frac{1}{\sqrt{\tau_l}}\frac{1}{\sqrt{\tau_c}}$, we have

$$\ln \tau_\alpha \approx \ln \bar{\tau}_l + \ln \bar{\tau}_c + \frac{\omega_l}{k_B T} + \left(\frac{\sigma_l}{k_B T}\right)^{n_l} + \frac{\omega_c}{k_B T}. \tag{8c}$$

Equation (8c), which covers all cases by properly choosing parameters, can be further simplified as

$$\ln \tau_\alpha \approx \ln \bar{\tau}_0 + \frac{\omega}{k_B T} + \left(\frac{\sigma_l}{k_B T}\right)^n, \tag{9}$$

where the parameters $\bar{\tau}_0$, ω, σ_l, and $n \leqslant 2$ are material dependent, respectively. Since $n \leqslant 2$, the dependence of the logarithm of the relaxation time on the reciprocal temperature cannot be higher than the second power or lower than the first power.

For $\rho_l(x)$, the Gaussian distribution may be a reasonable assumption, which is also used in previous models [13,15–17]. More importantly, some calculations also show the existence of a Gaussian-like distribution [28,63–67]. If $\rho_l(x) \sim \exp[-(\frac{x-\Delta}{2\sigma})^2]$ is a Gaussian distribution with the distribution width σ and the average barrier $\Delta \geqslant 0$, Eq. (9) becomes

$$\ln \tau_\alpha \approx \ln \bar{\tau}_0 + \frac{\omega}{k_B T} + \left(\frac{\sigma}{k_B T}\right)^2. \tag{10}$$

In this case, from Eqs. (8), we find that $\Delta \geqslant \omega \geqslant E_0 - \in_0$. Because of $E_0 - \in_0 \leqslant 0$, ω can be either positive or negative dependent on the relative importance of $\rho_l(x)$ and $\rho_c(x)$ (see below for details). Here ω reflects the effect barrier height contributed from both ρ_l and ρ_c, and σ refers the effect distribution width of ρ_l. Thus, ω and σ are mathematically independent and have dimensions of barrier height and distribution width, respectively. Hereafter ω and σ are labeled

as the effective barrier and the effective width of the DOB, respectively. Accordingly, the fragility becomes

$$m = \frac{d \log (\tau_\alpha)}{d(T_g/T)}\Big|_{T=T_g} = \frac{\omega}{k_B T_g} + 2\left(\frac{\sigma}{k_B T_g}\right)^2. \quad (11)$$

Equations (10) and (11) will be used in the following discussions.

According to Eq. (11), the fragility can be well interpreted within the PEL perspective. If $\rho_l(x)$ is a sharp and narrow distribution, i.e., the PEL is flat, the contribution from $\rho_c(x)$ may be neglected, and a strong glass is expected. In this case, the effective barrier ω will be positive. Conversely, if $\rho_l(x)$ is a very wide and flat distribution, i.e., a rough PEL, $\rho_c(x)$ begins to play a more and more important role, and the effective barrier ω tends to be negative, then a fragile glass is expected. The above correspondence between PEL roughness and fragility has been confirmed in previous simulations [29,41,45,65]. The shapes of $\rho_l(x)$ and $\rho_c(x)$ for the strong and fragile glass are sketched in the lower panel of Fig. 1.

Quite a few previous studies in particular have shown that the soft interactions or soft particles make strong glasses [68–71]. Here we can make a qualitative understanding for such connections between the fragility and the interaction potential. From Eq. (11), one can see that the key parameters affecting fragilities are ω and σ. Obviously, $\sigma \propto \frac{1}{\sqrt{B_l}}$ characterizes the distribution width of barriers. The larger B_l is, the smaller σ, while $\omega \sim \Delta + E_0 - E_i$ represents the energy difference. Although we cannot establish an explicit formula between the interaction potential and these parameters, a qualitative relationship can be obtained. As the interatomic potential becomes softer, the whole PEL will be squished, namely, become flatter and flatter. An extreme example is the ideal gas, whose PEL is flat. As a result, the DOB will become narrower (a larger B_l or a smaller σ), and any energy difference will be reduced (a smaller ω) accordingly. From Eq. (11), we can see that the smaller ω and σ result in a smaller fragility, which is in agreement with the statement of "soft particles making strong glasses." A more rigorous treatment will be published later.

If some fundamental changes have taken place in the effect DOB, the capability of our model opens for discussion. For example, upon cooling, most glasses undergo a fragile-to-strong crossover [72], which is believed to originate from the ergodicity breakdown. After the ergodicity breakdown, the system no longer "sees" the original DOB, thus our model may be no longer valid. In fact, we do find the fitting becomes poor after the fragile-to-strong crossover (see Appendix E).

A quadratic dependence of τ_α on temperature, similar to the form of Eq. (10), was discussed in previous papers, e.g., the Gaussian model and ECG model [9,13]. The Gaussian model does predict a quadratic dependence of τ_α on temperature $\tau = \tau_\infty \exp[(T_0/T)^2]$, where T_0 is a material-dependent characteristic temperature given by $k_B T_0 \propto \sigma_G$. Parameter σ_G here is the width of the Gaussian distribution. Though such quadratic dependence can be used to fit curves in AP, T_0 shows an increasing trend with decrease in fragility, indicating that the distribution of barriers in strong glasses is broader than that in fragile glasses, which is opposite to the results of previous simulations [29,41,45,65]. More importantly, if

the Gaussian form is adopted, a negative average barrier is obtained when fitting to fragile glasses (see Appendix E), which obviously cannot be the case. It is the existence of ρ_c in the current model that avoids the problem of a negative average barrier and guarantees a PEL of the fragile glasses being rougher than that of strong glasses.

In ECG model, to obtain the quadratic form, the authors have taken a class of kinetically constrained models, in which the barrier is correlated to a characteristic length scale. After simple mathematical processing, our model [Eq. (10)] can also be transformed into the ECG form $\ln(\frac{\tau}{\tau_o^*}) = J^2(\frac{1}{T} - \frac{1}{T_o})^2$, with $J^2 = \frac{\sigma^2}{k_B^2}$, $T_o = -2\frac{\sigma^2}{k_B^2 \omega}$, and $\ln(\frac{\bar{\tau}_o}{\tau_o^*}) = 4\frac{k_B^2 \omega^2}{\sigma^2}$. Here, to make the ECG equation meaningful, a negative ω must be assumed. If Eq. (10) is used to fit the AP, a positive (negative) ω will be obtained for typical strong (fragile) glasses. Obviously, if the ECG equation is used to describe strong glasses, a much lower T_o will be obtained, which evidently invalidates the physics meaning of T_o.

The current model can also be used to explain the results from various computer simulations, such as the square well (SqW) model. In SqW model, the interaction between atoms is described by an attractive square well with a tunable barrier (Δ) at its outer edge. It was found that, by increasing Δ, the system shows a trend from fragile to strong in dynamics without changing its thermodynamics fragility. Since the width of the barrier is infinitesimal compared to the size of particles and width of the well, when the observation time is much longer than the typical relaxation time, changing Δ has little effect on thermodynamics properties [33]. However, the increase of Δ in the SqW potential does affect the kinetic behavior. At a given temperature, there exists a threshold barrier height x_{th}, and the barriers above x_{th} are too high to be overcome. By increasing Δ, more barriers grow higher than x_{th} and fewer remain available for dynamics processes. Therefore, the effective DOB will become narrower as increasing Δ and results in the decrease of fragility. This result is in agreement with the prediction of our current model.

B. Comparison to molecular dynamics and experimental data

Tuning the PEL will be the most direct test of the current model. Recently we have proposed a MD method to adjust a PEL [73]. The advantage of this method is that it changes only the height of barriers in a PEL, but the number and position of minima in phase space are kept unchanged. Consider $\varphi(r_1, r_2, \ldots, r_N)$ being the total potential energy of a system, which defines the PEL of this system. In order to adjust the PEL, we define an alternative total potential energy φ^* as

$$\varphi^* = \begin{cases} \varphi + \varepsilon(\varphi - \varphi_a)^m, & for\ \varphi \leqslant \varphi_a \\ \varphi, & for\ \varphi > \varphi_a \end{cases}, \quad (12)$$

where ε and φ_a are adjustable parameters, and m is an even number ($m \geqslant 2$). Obviously, φ^* defines a different PEL. Here the negative parameter ε is used to tune the heights of barriers. When ε is reduced, all barriers will be raised accordingly, and thus DOB naturally becomes broader in comparison to that of the original PEL. Because the larger the energy difference is, the larger the degree of modification on PELs, the tuning will have a greater effect on $\rho_l(x)$ than on $\rho_c(x)$. Here this method
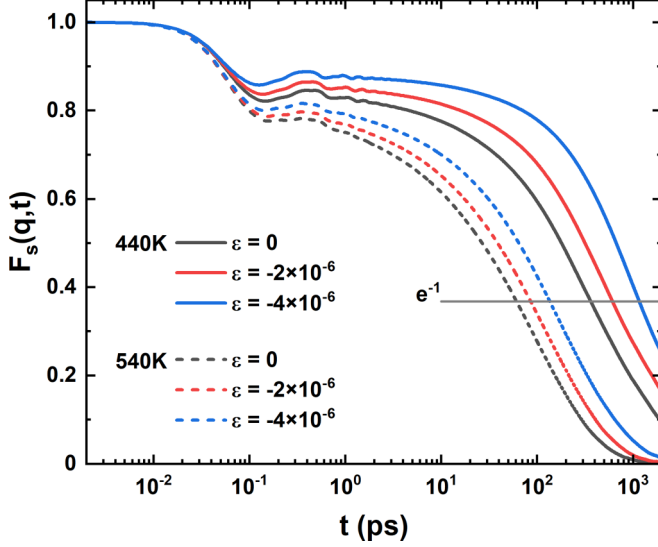
FIG. 2. Self-intermediate scattering function of Al_{46} at 440 K and 540 K for different ε. As ε is lowered, the structural relaxation time increases significantly.

has been employed to modify the PELs of two nanoglasses (Al_{43} and Al_{46} clusters). The relevant computational details are presented in Appendix D.

The self-intermediate scattering function (SISF) provides rich information on structural relaxations, which is shown in Fig. 2 for two selected temperatures. τ_{α} is given by the intersection of SISFs and the solid line (e^{-1}). It can be seen that, as the PEL becomes rougher (ε being lower), the structural relaxation does show a significant slowdown, and such a slowdown is more pronounced at low temperatures. This is easy to understand because the lower ε is, the higher barrier is.

The AP of Al_{43} and Al_{46}, in the upper panel of Fig. 3, in which T_{g} is determined according to τ_{α}, reaches the order of 100 ps. From this figure, one can see that, Al_{43} can be considered a strong glass former at $\varepsilon = 0$, indicated by the Arrhenius relation between τ_{α} and temperature. Al_{46} slightly deviates from the Arrhenius relation even at $\varepsilon = 0$, indicating a less strong behavior. With the decrease of ε, the τ_{α}-temperature curves begin to deviate from the Arrhenius relation, indicating the system tends to be more fragile. This result is actually the most direct support of both our model and previous speculation, namely, that the PEL of a fragile glass is "rougher," because in our current work, as the PEL is adjusted, only barriers are changed. The τ_{α}-temperature curves from our MD simulations can be well fitted by Eq. (10), as shown in the upper panel of Fig. 3. Besides our MD data, Eq. (10) well describes the τ_{α}-temperature curves of various glasses perfectly. Here the experimental results are taken from Refs. [74–83]. The lower panel of Fig. 3 presents the selected fitted results of the relaxation time by Eq. (10), which is almost perfectly fitted. More fitting results for these experimental works are presented in Appendix E.

The fitting parameters ($\bar{\tau}_0$, ω, and σ) for Al_{43} and Al_{46} are listed in Table I, from which it is seen that our model gives a clear physical description of APs. With decreasing ε, ω decreases and σ increases accordingly. Such a trend is in line with our expectations, since the PEL becomes rougher as ε de-
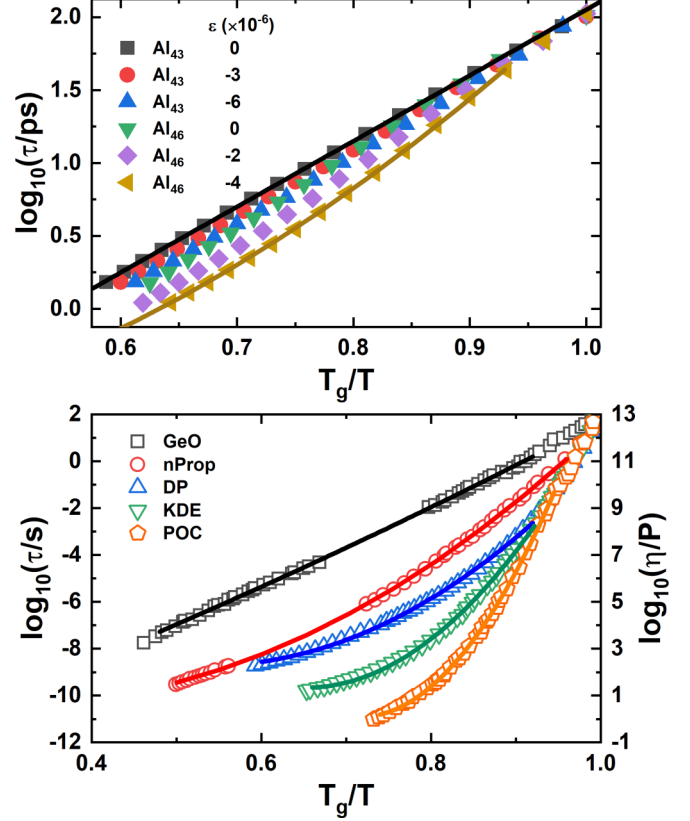

FIG. 3. Upper panel: The Angell plot of Al_{43} and Al_{46} nanoglasses. With the decrease of ε, the τ_{α}-temperature curves gradually deviate from the Arrhenius form, indicating the trend to be fragile. Lower panel: The Angell plot for various glasses adopted from experimental work. Lines are the fitting results based on Eq. (10). Both the experimental data and the current molecular dynamics data can be well fitted by Eq. (10).

creases. Correspondingly, the system becomes more and more fragile, the effective barrier ω does not increase but decreases. This indicates that $\rho_c(x)$ begins to play a nonnegligible role. At the same time, σ grows larger. As discussed above, σ is a parameter positively correlated with the effective width of $\rho_c(x)$. The manipulation of the PEL enlarges the difference between barriers, and therefore leads to the increase of σ. Similar trends between ω and σ are also observed in other glasses (see Table II in Appendix E). The above discussion gives us a strong hint that there could be a special relationship between ω and σ.

TABLE I. The parameters ($\bar{\tau}_0$, ω, σ) obtained for nanoglasses by fitting MD data with Eq. (10).

System	ε ($\times 10^{-6}$)	$\ln \bar{\tau}_0$	ω (eV)	σ^2 ($\times 10^{-2}\mathrm{eV}^2$)
Al_{43}	0	−5.65	0.42	0
	−3	−5.08	0.34	0.25
	−6	−4.60	0.27	0.51
Al_{46}	0	−5.91	0.38	0.36
	−2	−4.64	0.20	1.02
	−4	−2.71	−0.15	2.2
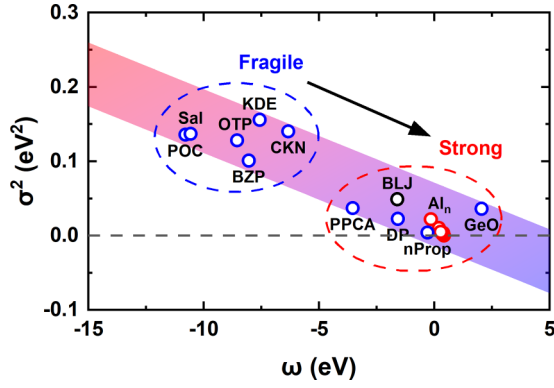
FIG. 4. σ^2 as a function of ω for various glasses. ω and σ^2 seem to have a simple linear relationship. All glasses are distributed in a narrow band. The purple area marks this band, in which the direction of the arrow shows the trend of fragility from fragile towards strong.

By fitting various glass-forming liquids from polymers, metal alloys to molten salts, and nano- to bulk glasses, we find a simple linear relationship between ω and σ^2, as shown in Fig. 4. In this figure, the current MD results for the binary Lennard-Jones system (black open circle) and nanoglasses (red open circles) are also included. From this figure, one can see that σ^2 increases with the decrease of ω. More importantly, ω and σ^2 exhibit a linear relationship. All glasses are distributed in a very narrow band, in which fragile and strong glasses locate in the upper left and lower right regions, respectively, in line with our theoretical expectation discussed above.

The narrow-band distribution in Fig. 4 implies that glasses or glass transitions may occur only for a restricted category of PELs, namely, within a certain range of ω and σ^2. It is not too difficult to argue that far away from this band the glassy state would not exist. Considering two parts that contribute to it, i.e., ω_l and ω_c, ω shall have both a maximum and a minimum. On one hand, a large value of ω corresponds to high local barriers ω_l, which would prevent the system from relaxing towards lower MBs. On the other hand, remember that $\omega \geqslant E_0 - \epsilon_0$ (the difference between the ground-state energy of systems and the zero-temperature energy of the glass), and ω cannot be infinitely small, otherwise the system would be unstable. In fact, although the glassy state is metastable, it could not have a very high energy compared to the ground-state energy. What's more, in the ω-σ^2 plot, we find another intriguing feature, namely, that the typical fragile and strong (or weak fragile) glasses are well separated. Thus, we can see that the so-called fragile and strong glasses are really different from the perspective of PELs.

III. CONCLUSION

We have established a model for α relaxation based on the potential energy landscape perspective. We find that the Angell plot can be well explained as long as the barrier distribution is reasonably described. The key issue in our model is to realize that the total distribution of barriers is divided in two parts: a local Gaussian-like distribution and an extended power-law distribution. Our model shows that a fragile glass tends to have a wide, Gaussian-like distribution, while a strong glass tends to have a narrow Gaussian-like distribution. By comparing various glass systems, we find that these glasses are distributed in a very narrow band determined by two parameters, the square of the effective width of the Gaussian-like distribution and the effective barrier.

APPENDIX A: MATHEMATICAL DERIVATION OF $\rho_l(x)$

Let $\Omega(E)$ be the number of states with energy E, and the entropy expressed as $k_B \ln[\Omega(E)]$. According to statistical physics, $\Omega(E)$ can be calculated as

$$\Omega(E) = \left(\frac{1}{2\pi\hbar}\right)^{3N} \int \delta(E - [H(\{q_i, q_i\}) - E_0]) \prod_i dq_i dq_i,$$
(A1)

where q_i and p_i are the coordinate and momentum of the ith atom, respectively. N and H are the total number of atoms and the total energy for a given $\{q_i, q_i\}$, respectively, and E_0 is the energy of the ground state. In classical physics, the number of states cannot be well counted. To roughly estimate the number of states around the energy E, the total energy H is formally written as the sum of energies of N atoms, namely,

$$H(\{q_i, q_i\}) - E_0 = \sum_i^N h_i.$$
(A2)

Accordingly, Eq. (A2) can be rewritten as

$$\Omega(E) \propto \frac{1}{N!} \int \delta\left(E - \sum_i^N h_i\right) \prod_i^N g(h_i) dh_i,$$
(A3)

where $g(h_i)$ counts the degeneracy at h_i or the reciprocal of energy-level spacing. For the ideal gas, $g(h_i) \propto h_i^{1/2}$; for the three-dimensional harmonic oscillator, $g(h_i) \propto h_i^2$; for the one-dimensional harmonic oscillator, $g(h_i)$ is a constant. Generally speaking, the higher the energy, the narrower the energy level spacing, and the larger $g(h_i)$. Without losing generality, we write $g(x)$ in the form of x^{B_c}, where B_c is a constant for a given system. Then we have

$$\Omega(E) \propto \frac{1}{N!} \int \delta\left(E - \sum_i^N h_i\right) \prod_i^N h_i^{B_c} dh_i.$$
(A4)

By variable substitutions, $h_i = y_i^2$, we have

$$\Omega(E) \propto \frac{2^N}{N!} \int \delta\left(E - \sum_i^N y_i^2\right) \prod_i^N y_i^{2B_c+1} dy_i.$$
(A5)

This integral can be easily performed in spherical coordinates. By writing $Y^2 = \sum_i^N y_i^2$, we obtain

$$\Omega(E) \propto \mathbb{C} \frac{2^N}{N!} \int \delta(E - Y^2) Y^{2NB_c+N} Y^{N-1} dR$$

$$= \frac{2^{N-1}}{N!} E^{N(B_c+1)-1}.$$
(A6)

$\mathbb{C}$ is a constant containing the integration over angles, which is irrelevant to our discussion. Through simple mathematical deduction, we arrive at the final formula,

$$\Omega(E) = R_c \left(\frac{E}{N}\right)^{NB_c}. \tag{A7}$$

In Eq. (A1) we have set the zero point of energy at the ground state. If we change the zero point of energy back to its original position, Eq. (A7) will become Eq. (2). One can see that both R_c and B_c are material dependent, since they depend on the specific expression of $g(h_i)$.

APPENDIX B: MATHEMATICAL DEDUCTION FOR THE CONTRIBUTION FROM $\rho_l(x)$

Considering $f(x) = B_l(x-\Delta)^n \geqslant 0.0$ and $\rho_l(x) = R_l e^{-f(x)}$, where B_l, R_l, Δ, and n are constants larger than zero. Defining $F(x) = -\beta x - f(x)$, then $\rho_l(x)e^{-\beta x} = e^{-\beta x - f(x)} = e^{F(x)}$ should be a fast-decayed function of x. Namely, it is important only in the vicinity of the maximum of $F(x)$. Thus, it is reasonable to replace $F(x)$ by its Taylor expansion,

$$F(x) \cong -\beta\bar{x} - f(\bar{x}) - \frac{1}{2}f''(\bar{x})(x-\bar{x})^2 + O(3), \tag{B1}$$

where $\bar{x}$ is determined by $\frac{\partial F}{\partial x}\big|_{\bar{x}} = 0$. Then

$$\frac{1}{\tau_l} = \frac{R_l}{\tau_0} \int e^{-\beta\bar{x} - f(\bar{x}) - \frac{1}{2}f''(\bar{x})(x-\bar{x})^2 + O(3)}$$

$$\approx \frac{R_l}{\tau_0}\sqrt{\frac{2\pi}{f''(\bar{x})}}e^{-\beta\bar{x} - f(\bar{x})}. \tag{B2}$$

Now taking $f(x) = B_l(x-\Delta)^n$, we have

$$\bar{x} = \Delta - \left(\frac{\beta}{nB_l}\right)^{\frac{1}{n-1}}, \tag{B3a}$$

$$f''(\bar{x}) = n(n-1)B_l\left(\frac{\beta}{nB_l}\right)^{\frac{n-2}{n-1}}, \tag{B3b}$$

$$f(\bar{x}) = B_l\left(\frac{\beta}{nB_l}\right)^{\frac{n}{n-1}}. \tag{B3c}$$

After simple mathematical simplification, Eq. (B2) becomes

$$\frac{1}{\tau_l} \approx \frac{R_l}{\tau_0}\sqrt{\frac{2\pi}{f''(\bar{x})}}e^{-\frac{\Delta}{k_BT} + (n-1)B_l\left(\frac{1}{nB_lk_BT}\right)^{\frac{n}{n-1}}}. \tag{B4}$$

In order to make $f(x)$ physically meaningful, two constraints are needed. First, the second derivative of $f(x)$ ($f''(\bar{x})$) must be positive, it requires $n > 1$. This, of course, is consistent with that $\rho(x)$ must decay faster than $e^{\beta x}$ for larger x. Second, $f''(\bar{x})$ must increase with T, otherwise the fluctuation of τ_l will reach the largest at zero temperature, which obviously makes no sense. This condition requires $n \geqslant 2$.

APPENDIX C: MATHEMATICAL DEDUCTION FOR THE CONTRIBUTION FROM $\rho_c(x)$

Consider $\rho_c(x) = R_c\left(\frac{x+E_i-E_0}{\mathbb{N}}\right)^{B_cN} = R_c e^{g(x)}$ with $g(x) = B_cN\ln\left(\frac{x+E_i-E_0}{\mathbb{N}}\right)$, where $\mathbb{N}$, R_c, B_c, and E_0 are constants for a given glass, and $E_i \geqslant E_0$. Defining $G(x) = -\beta x + g(x)$,

then $\rho_c(x)e^{-\beta x} = e^{-\beta x + g(x)} = e^{G(x)}$ should be a fast-decayed function of x. Namely, it is important only in the vicinity of the maximum of $G(x)$. Thus, it is reasonable to replace $G(x)$ by its Taylor expansion,

$$G(x) \cong -\beta\bar{x} + g(\bar{x}) + \frac{1}{2}g''(\bar{x})(x-\bar{x})^2 + O(3), \tag{C1}$$

where $\bar{x}$ is determined by $\frac{\partial G}{\partial x}\big|_{\bar{x}} = 0$; thus

$$\bar{x} = E_0 - E_i + \frac{B_cN}{\beta}, \tag{C2a}$$

$$g(\bar{x}) = B_cN\ln\left(\frac{B_cN}{\mathbb{N}\beta}\right), \tag{C2b}$$

$$g''(\bar{x}) = -NB_c\left(\frac{B_cN}{\beta}\right)^{-2}. \tag{C2c}$$

After mathematical simplification, Eq. (3c) becomes

$$\frac{1}{\tau_c} = \frac{R_c}{\tau_0}\int e^{-\beta\bar{x} + g(\bar{x}) + \frac{1}{2}g''(\bar{x})(x-\bar{x})^2 + O(3)}$$

$$\approx \frac{R_c}{\tau_0}\sqrt{\frac{2\pi}{|g''(\bar{x})|}}e^{-\beta\bar{x} + g(\bar{x})}, \tag{C3}$$

where

$$-\beta\bar{x} + g(\bar{x}) = \beta(E_i - E_0) + B_cN + B_cN\ln\left(\frac{B_cN}{\mathbb{N}\beta}\right). \tag{C4}$$

Then

$$\frac{1}{\tau_c} \approx \frac{R_c}{\tau_0}\sqrt{\frac{2\pi}{|g''(\bar{x})|}}e^{\frac{E_i}{k_BT} - \frac{E_0}{k_BT} + B_cN + B_cN\ln\left(\frac{B_cN}{\mathbb{N}\beta}\right)}. \tag{C5}$$

To make $g(x)$ have physical meaning, similar to that for $g(x)$, two constraints are needed. The second derivative of (x) [$g''(\bar{x})$] must be negative and decrease with T, which are automatically satisfied.

APPENDIX D: COMPUTATONAL METHODS

The thermodynamics behavior of two aluminum nanoclusters (Al_{43} and Al_{46}) were studied, and the empirical potential was adopted to describe the atomic interaction of Al[18]. The constant temperature MD method without any boundary conditions was used in the calculations. At each temperature of interest, a 10 ns simulation for initial relaxation is performed, followed by a $6\,\mu$s simulation. Previous studies had shown that both Al_{43} and Al_{46} have a disordered structure at its ground state and melt or solidify with a typical glasslike transition, namely, the continuous change in energy and volume [60,73].

To manipulate PELs, the method developed by some of us was used. Here the key points were listed as follows: the high-dimensional PELs are the function of the total potential energy of systems (*note:* the total potential energy is not the interatomic potential). Suppose $\varphi(\boldsymbol{r}_1, \boldsymbol{r}_2, \ldots, \boldsymbol{r}_N)$ being the total potential energy function, an alternative total potential energy φ^* is defined as

$$\varphi^* = \begin{cases} \varphi + \varepsilon(\varphi - \varphi_a)^m, & for\ \varphi \leqslant \varphi_a \\ \varphi, & for\ \varphi > \varphi_a \end{cases}, \tag{D1}$$

where ε, φ_a, and m are adjustable parameters. It can be easily demonstrated that, by proper choice of ε, φ_a, and m, the PEL

FIG. 5. Fitting MD results with Eq. (10).

FIG. 6. Fitting experimental results with Eq. (10).
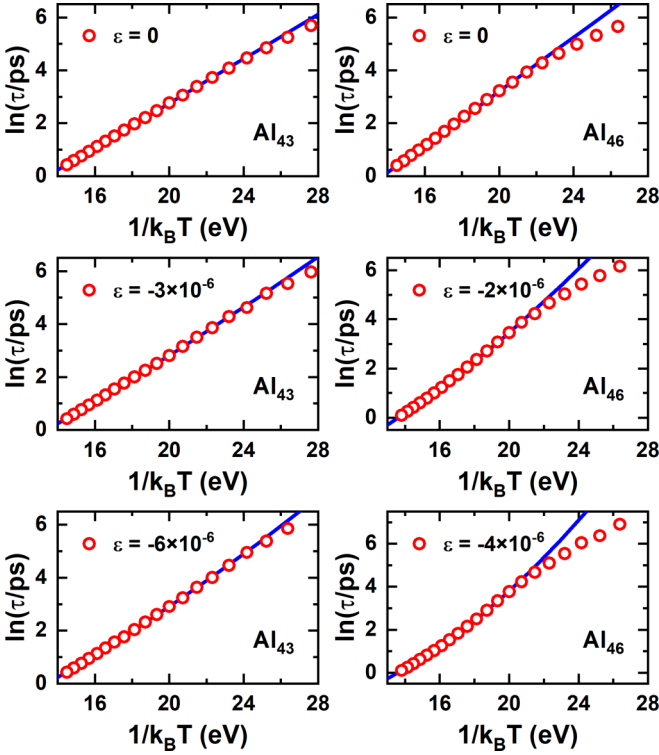
determined by φ^* has the adjustable barriers but the same topologic structure as the one determined by φ. Namely, by adjusting PELs, both the number and position of extreme points in phase space is unchanged, but only the height of barriers or the roughness of PELs are modified, which is a remarkable feature of our method. In current studies, for Al$_{43}$ (Al$_{46}$), φ_a and m were $-2.58 \times 43(46)$ eV and 6, respectively. And ε was chosen in the range of $[-6 \times 10^{-6}, 0]$. Since here ε is negative, the PEL becomes steeper as ε is decreased; in other words, the fluctuation of barriers increases.

To obtain the structural relaxation time (the so-called α-relaxation time, τ_α), the self-intermediate scattering function (SISF), which reveals a stretched time evolution of structure, is calculated by

$$F_s(q, t) = N^{-1} \left\langle \sum_{i=1}^{N} \exp\{i\boldsymbol{q} \cdot [\boldsymbol{r}_i(0) - \boldsymbol{r}_i(t)]\} \right\rangle, \quad \text{(D2)}$$

where N is the number of atoms in nanoclusters, $\langle \, \rangle$ denotes the ensemble average, and $\boldsymbol{q}$ is the wave vector. In this work, $|\boldsymbol{q}| = q_{\max} = 2.84$ Å^{-1}, i.e., the position of the main peak in the static structure factor $S(q)$ [84]. From SISF, one can obtain the structural relaxation time τ_α, which is usually defined as $F_s(q, t = \tau_\alpha) = e^{-1}$.

APPENDIX E: FITTING TO MD AND EXPERIMENTAL DATA

The fitting curves to MD and experimental data using Eq. (10) are shown in Fig. 5 and Fig. 6, respectively. The fitting parameters for different glass-forming materials are listed in Table II. In many glass formers there exists such a fragile-strong crossover, i.e., at the low-temperature region, that the temperature dependence of structural relaxation time and viscosity shows a non-Arrhenius to Arrhenius crossover, which is thought to be connected to the breakdown of ergodicity. Due to the broken ergodicity, the system no longer "sees" the complete distribution of barriers, so the relationship does not hold below the crossover temperature; see, for example, the fitting curves to Al$_{46}$ in Fig. 5, and BZP and CKN in Fig. 6.

TABLE II. The parameters ($\bar{\tau}_0$, ω, σ) obtained by fitting experimental results with Eq. (10).

System	Full name	ln (τ_0)	ln(η_0)	ω (eV)	$\sigma^2 (\times 10^{-2} \text{eV}^2)$	Ref.
GeO	GeO$_2$		-7.01	2.05	3.61	[74]
nProp	n-propanol	-18.41		-0.29	0.40	[75]
DP	Dibutyl-phthalate	7.70		-1.58	2.26	[76]
KDE	Cresolphthalein-dimethylether	69.69		-7.57	15.58	[77]
Sal	Salol	182.48		-10.56	13.68	[78]
OTP	o-terphenyl	120.32		-8.55	12.83	[79]
PPCA	Propylene carbonate	61.79		-3.54	3.70	[80]
CKN	Ca$-$K$-$NO$_3$	46.34		-6.33	14.03	[81]
BZP	Benzophenone	138.75		-8.05	10.10	[82]
POC	α-phenyl-o-cresol		214.37	-10.79	13.58	[83]

[1] C. A. Angell, Science **267**, 1924 (1995).
[2] M. Micoulaut, Rep. Prog. Phys. **79**, 066504 (2016).
[3] D. L. Sidebottom, J. NonCryst. Solids **524**, 119641 (2019).
[4] S. Sastry, Nature (London) **409**, 164 (2001).
[5] H. Vogel, Phys. Z. **22**, 645 (1921).
[6] G. S. Fulcher, J. Am. Ceram. Soc. **8**, 339 (1925).
[7] G. Tammann and G. Hesse, Z. Anorg. Allg. Chem. **156**, 245 (1926).
[8] G. Adam and J. H. Gibbs, J. Chem. Phys. **43**, 139 (1965).
[9] Y. S. Elmatad, D. Chandler, and J. P. Garrahan, J. Phys. Chem. B **114**, 17113 (2010).
[10] J. C. Mauro, Y. Yue, A. J. Ellison, P. K. Gupta, and D. C. Allan, Proc. Natl. Acad. Sci. USA **106**, 19780 (2009).
[11] B. A. Pazmiño Betancourt, P. Z. Hanakata, F. W. Starr, and J. F. Douglas, Proc. Natl. Acad. Sci. USA **112**, 2966 (2015).
[12] C. A. Angell, K. L. Ngai, G. B. McKenna, P. F. McMillan, and S. W. Martin, J. Appl. Phys. **88**, 3113 (2000).
[13] H. Bässler, Phys. Rev. Lett. **58**, 767 (1987).
[14] P. M. Derlet and R. Maaß, Philos. Mag. **94**, 2776 (2014).
[15] M. Ikeda and M. Aniya, J. NonCryst. Solids **371–372**, 53 (2013).
[16] M. Ikeda and M. Aniya, J. Alloys Compd. **805**, 904 (2019).
[17] T. A. Vilgis, J. Phys. Condens. Matter **2**, 3667 (1990).
[18] C. S. Lee, M. Lulli, L. H. Zhang, H. Y. Deng, and C. H. Lam, Phys. Rev. Lett. **125**, 265703 (2020).
[19] J. C. Dyre, Phys. Rev. B **51**, 12276 (1995).
[20] A. Baronchelli, A. Barrat, and R. Pastor-Satorras, Phys. Rev. E **80**, 020102(R) (2009).
[21] C. Rehwald and A. Heuer, Phys. Rev. E **86**, 051504 (2012).
[22] Y. Fan, T. Iwashita, and T. Egami, Nat. Commun. **8**, 15417 (2017).
[23] R. G. Margiotta, R. Kühn, and P. Sollich, J. Stat. Mech. (2019) 093304.
[24] F. H. Stillinger, Science **267**, 1935 (1995).
[25] S. Sastry, P. G. Debenedetti, and F. H. Stillinger, Nature (London) **393**, 554 (1998).
[26] S. Büchner and A. Heuer, Phys. Rev. Lett. **84**, 2168 (2000).
[27] D. J. Wales and J. P. K. Doye, Phys. Rev. B **63**, 214204 (2001).
[28] T. F. Middleton and D. J. Wales, Phys. Rev. B **64**, 024205 (2001).
[29] A. J. Moreno, S. V. Buldyrev, E. La Nave, I. Saika-Voivod, F. Sciortino, P. Tartaglia, and E. Zaccarelli, Phys. Rev. Lett. **95**, 157802 (2005).
[30] A. Saksaengwijit and A. Heuer, Phys. Rev. E **73**, 061503 (2006).
[31] V. K. De Souza and D. J. Wales, J. Chem. Phys. **130**, 194508 (2009).
[32] S. Banerjee and C. Dasgupta, Phys. Rev. E **85**, 021501 (2012).
[33] A. D. Parmar and S. Sastry, J. Phys. Chem. B **119**, 11243 (2015).
[34] G. Ruocco, F. Sciortino, F. Zamponi, C. De Michele, and T. Scopigno, J. Chem. Phys. **120**, 10666 (2004).
[35] U. Buchenau, J. Phys. Condens. Matter **15**, S955 (2003).
[36] R. A. Denny, D. R. Reichman, and J.-P. Bouchaud, Phys. Rev. Lett. **90**, 025503 (2003).
[37] M. Goldstein, J. Chem. Phys. **51**, 3728 (1969).
[38] F. Sciortino, J. Stat. Mech. (2005) P05015.
[39] A. Heuer, J. Phys. Condens. Matter **20**, 373101 (2008).
[40] Z. Raza, B. Alling, and I. A. Abrikosov, J. Phys. Condens. Matter **27**, 293201 (2015).
[41] S. Yip, Mol. Simul. **42**, 1330 (2016).
[42] F. H. Stillinger and T. A. Weber, Phys. Rev. A **25**, 978 (1982).
[43] P. G. Debenedetti and F. H. Stillinger, Nature (London) **410**, 259 (2001).
[44] B. Doliwa and A. Heuer, Phys. Rev. E **67**, 031506 (2003).
[45] B. Doliwa and A. Heuer, Phys. Rev. Lett. **91**, 235501 (2003).
[46] Y. Yang and B. Chakraborty, Phys. Rev. E **80**, 011501 (2009).
[47] R. Golovchak, A. Kovalskiy, O. Shpotyuk, and H. Jain, Appl. Phys. Lett. **98**, 171905 (2011).
[48] J. S. Bender, M. Zhi, and M. T. Cicerone, Soft Matter **16**, 5588 (2020).
[49] G. A. Appignanesi, J. A. Rodríguez Fris, R. A. Montani, and W. Kob, Phys. Rev. Lett. **96**, 057801 (2006).
[50] M. Goldstein, J. Chem. Phys. **132**, 041104 (2010).
[51] R. G. Palmer, D. L. Stein, E. Abrahams, and P. W. Anderson, Phys. Rev. Lett. **53**, 958 (1984).
[52] W. H. Wang, Prog. Mater Sci. **106**, 100561 (2019).
[53] S. K. Ma, *Statistical Mechanics* (World Scientific, Singapore, 1985).
[54] D. J. Wales and J. P. K. Doye, J. Chem. Phys. **119**, 12409 (2003).
[55] M. S. Shell, P. G. Debenedetti, and A. Z. Panagiotopoulos, Phys. Rev. Lett. **92**, 035506 (2004).
[56] L. Berthier, M. Ozawa, and C. Scalliet, J. Chem. Phys. **150**, 160902 (2019).
[57] F. H. Stillinger, Phys. Rev. E **59**, 48 (1999).
[58] T. F. Middleton and D. J. Wales, J. Chem. Phys. **118**, 4583 (2003).
[59] J. Chowdhary and T. Keyes, J. Phys. Chem. B **108**, 19786 (2004).
[60] D. M. Zhang, D. Y. Sun, and X. G. Gong, Phys. Rev. B **105**, 035403 (2022).
[61] R. Faller and J. J. De Pablo, J. Chem. Phys. **119**, 4405 (2003).
[62] J. C. Martinez-Garcia, S. J. Rzoska, A. Drozd-Rzoska, and J. Martinez-Garcia, Nat. Commun. **4**, 1823 (2013).
[63] A. Heuer, Phys. Rev. Lett. **78**, 4051 (1997).
[64] J. Bewerunge and S. U. Egelhaaf, Phys. Rev. A **93**, 013806 (2016).
[65] H. Kallel, N. Mousseau, and F. Schiettekatte, Phys. Rev. Lett. **105**, 045503 (2010).
[66] Y.-B. Yang, Q. Yang, D. Wei, L.-H. Dai, H.-B. Yu, and Y.-J. Wang, Phys. Rev. B **102**, 174103 (2020).
[67] S. Zhang, C. Liu, Y. Fan, Y. Yang, and P. Guan, J. Phys. Chem. Lett. **11**, 2781 (2020).
[68] J. Mattsson, H. M. Wyss, A. Fernandez-Nieves, K. Miyazaki, Z. Hu, D. R. Reichman, and D. A. Weitz, Nature (London) **462**, 83 (2009).
[69] J. Krausser, K. H. Samwer, and A. Zaccone, Proc. Natl Acad. Sci. USA **112**, 13762 (2015).
[70] J. Krausser, A. E. Lagogianni, K. Samwer, and A. Zaccone, Phys. Rev. B **95**, 104203 (2017).
[71] P. Lunkenheimer, F. Humann, A. Loidl, and K. Samwer, J. Chem. Phys. **153**, 124507 (2020).
[72] F. Mallamace, C. Branca, C. Corsaro, N. Leone, J. Spooren, S. H. Chen, and H. E. Stanley, Proc. Natl Acad. Sci. USA **107**, 22457 (2010).
[73] D. Y. Sun and X. G. Gong, New J. Phys. **22**, 103020 (2020).
[74] A. Sipp, Y. Bottinga, and P. Richet, J. NonCryst. Solids **288**, 166 (2001).
[75] R. Richert and C. A. Angell, J. Chem. Phys. **108**, 9016 (1998).

[76] P. K. Dixon, L. Wu, S. R. Nagel, B. D. Williams, and J. P. Carini, Phys. Rev. Lett. **65**, 1108 (1990).

[77] M. Paluch, K. L. Ngai, and S. Hensel-Bielowka, J. Chem. Phys. **114**, 10872 (2001).

[78] Y. Yang and K. A. Nelson, J. Chem. Phys. **103**, 7732 (1995).

[79] W. Steffen, A. Patkowski, G. Meier, and E. W. Fischer, J. Chem. Phys. **96**, 4171 (1992).

[80] F. Stickel, E. W. Fischer, and R. Richert, J. Chem. Phys. **104**, 2043 (1996).

[81] Y. Yang and K. A. Nelson, J. Chem. Phys. **104**, 5429 (1996).

[82] P. Lunkenheimer, L. C. Pardo, M. Köhler, and A. Loidl, Phys. Rev. E **77**, 031506 (2008).

[83] W. T. Laughlin and D. R. Uhlmann, J. Phys. Chem. **76**, 2317 (1972).

[84] W. Kob and H. C. Andersen, Phys. Rev. E **52**, 4134 (1995).